

Channel flow in a Langmuir monolayer: Unusual velocity profiles in a liquid-crystalline mesophase

M. L. Kurnaz and D. K. Schwartz*

Department of Chemistry, Tulane University, New Orleans, Louisiana 70118

(Received 24 January 1997; revised manuscript received 9 June 1997)

We have observed the surface-pressure driven flow of an arachidic (eicosanoic) acid Langmuir monolayer through a narrow channel using Brewster angle microscopy. By following distinctive features of the monolayer domain morphology we determined the velocity profile across the channel for various values of surface pressure over a wide range of flow rates. At low surface pressure within the L_2 mesophase, the velocity profile is parabolic for low flow rates. This implies that the surface viscosity dominates the coupling to the aqueous subphase as a source of dissipation and that the monolayer behaves as a Newtonian fluid. At extremely high shear rates, a flattened velocity profile is observed, similar to plug flow. At higher surface pressure (≥ 20 mN/m) the velocity profile is again parabolic for low flow rates. However, as the flow rate is increased the velocity profile is observed to gradually sharpen, eventually becoming triangular. The critical shear rate for the onset of this flow profile is 0.2 s^{-1} . In a typical fluid, such a profile would indicate shear thickening. However, measurement of the surface pressure drop along the channel versus flow rate indicates that macroscopic surface viscosity actually decreases with shear rate in this regime. The sharp change in interfacial rheology at $\pi = 20$ mN/m suggests the presence of a monolayer phase transition. [S1063-651X(97)14409-9]

PACS number(s): 68.10.Et, 47.50.+d

INTRODUCTION

The flow of surfactant molecules at interfaces is important to the understanding of rheology and stability in multiphase materials with large interfacial area such as foams and emulsions [1]. In addition, many industrial processes involve interfacial flow, such as coating and spraying technologies. Moreover, because of the simplified two-dimensional geometry and the large degree of thermodynamic and conformational control that can be exerted on the constituent molecules, monolayers of insoluble amphiphiles (Langmuir monolayers) stand to serve as important model systems for the basic understanding of complex rheological behavior, such as non-Newtonian viscous response and multiphase flow.

A number of inventive methods have been developed for the measurement of surface shear viscosity, e.g., the canal viscometer [2,3], torsion disk viscometer [4–6], knife-edge viscometer, etc. Intriguing methods based on the motion of a sphere [7] or a needle [8] floating on the surface have been recently described. These various methods differ in the degree of sensitivity, however all give quantitative values of surface shear viscosity (often with the help of some assumptions and approximations). Our observations of the monolayer velocity profile across a narrow channel, in conjunction with the measurement of the surface pressure drop over the length of the channel, give quantitative values of surface viscosity only for large viscosity or high flow rates. However, they provide direct, unambiguous proof of novel non-Newtonian viscous response without the necessity of perturbing the surface with foreign bodies. In addition, measurement of surface viscosity alone would give no hint

of the unusual rheological behavior implied by the sharpening of the velocity profile. Our results, along with work by Fuller's group [9], regarding the influence of flow on molecular alignment, illustrate the importance of direct flow visualization in conjunction with measurement of surface viscosity (and elasticity).

We force the monolayer through a narrow channel by creating a surface pressure gradient along the channel (Marangoni flow). In general, one must consider both the viscosity within the monolayer and the drag exerted on the monolayer by viscous coupling to the underlying aqueous subphase. In previous work [10], we observed the flow (using fluorescence microscopy) of a pentadecanoic acid monolayer in a region of its phase diagram (L_2/L_1 coexistence) in which the surface viscosity is very low because it is dominated by the viscosity of the two-dimensional liquid L_1 phase. We showed that, for the geometry of our channel, if the surface viscosity is negligible compared to the subphase viscosity, the velocity profile across the channel should be semielliptical, exactly as we measured. Of course, in the opposite extreme, if the subphase viscosity can be ignored, then the system is reduced to the classical two-dimensional Poiseuille flow problem which gives a parabolic velocity profile for a Newtonian surface film. An exact solution of the problem for arbitrary ratios of surface to bulk viscosity by Stone [11] found a gradual evolution from a semielliptical to a parabolic profile.

In the current work, we use Brewster angle microscopy (BAM) [12,13] instead of fluorescence microscopy to visualize the flow. This allows us to extend our observations into the condensed region of the fatty acid monolayer phase diagram that contains a number of liquid-crystalline mesophases [14]. The surface viscosity is significantly greater than in the L_1 phase, therefore we do not observe the semielliptical profile associated with the influence of subphase drag. However,

*Electronic address: dks@mailhost.tcs.tulane.edu

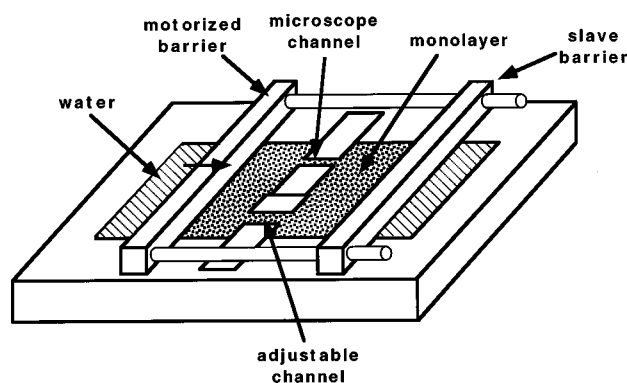


FIG. 1. Schematic diagram of the experimental trough apparatus showing the monolayer confined in the area between motorized and slave barriers. By moving the coupled barriers, the monolayer is forced through the channels in the middle barrier. The flow rate in the microscope channel is adjusted by a combination of the barrier speed and the width of the adjustable channel.

under certain thermodynamic conditions we observe velocity profiles that clearly indicate non-Newtonian viscous response.

EXPERIMENTAL DETAILS

Arachidic acid, $\text{CH}_3(\text{CH}_2)_{18}\text{COOH}$ (>99%, Sigma), was deposited from chloroform (Fisher Spectranalyzed) solution onto the surface of water (Millipore Milli-Q UV+) contained in a custom built Teflon Langmuir trough. The pH of the pure water in equilibrium with atmospheric CO_2 was 5.7 ± 0.1 . The temperature of the subphase was controlled to within ± 0.1 K using a combination of a recirculating water bath and thermoelectric Peltier elements and monitored with a Teflon encapsulated thermocouple probe. The surface pressure was measured using a filter paper Wilhelmy plate and an R&K electrobalance.

The trough was equipped with one motor-driven Teflon barrier and a second “slave” barrier that could be clamped in place to allow monolayer compression, or mechanically linked to the motorized barrier to allow the translation of the entire monolayer without compression (see Fig. 1). Between these two Teflon barriers was placed a stationary barrier made of glass and hydrophobized by treatment with octadecyltrichlorosilane. The glass barrier incorporated two channels 25 mm in length, one approximately 1 mm wide which was used for flow visualization using BAM, and a second with a variable width, 0–10 mm. The purpose of the second channel was to create a two-dimensional “flow divider” to permit the control of particularly low flow rates through the microscope channel. After bringing the monolayer to the desired surface pressure and temperature, the slave barrier was coupled to the motorized barrier and the monolayer was forced through the channels in the stationary glass barrier by slowly moving the motorized barriers in concert. The flow rate was varied by a combination of the motor speed (in combination with a series of timing belts and pulleys) and the ratio of the flow divider. The surface pressure drop along the channel was determined by independently measuring the surface pressure on the high and low pressure sides of the channel during monolayer flow at locations far from the en-

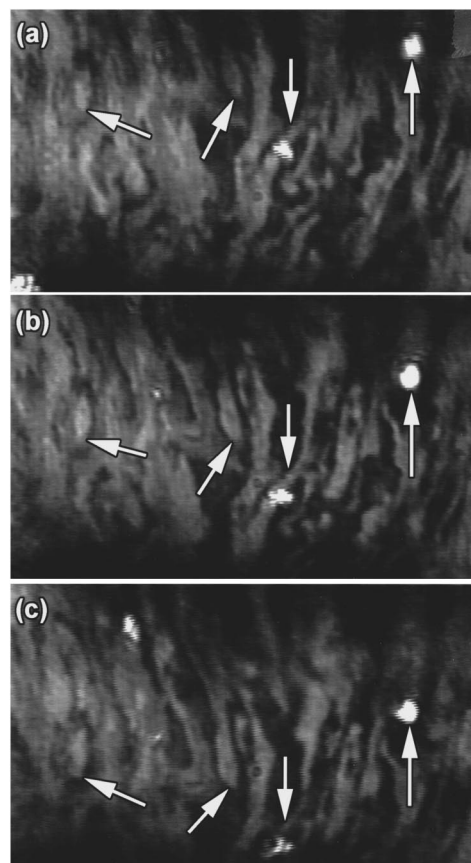


FIG. 2. (a)–(c) A typical sequence of BAM images during arachidic acid monolayer flow from top to bottom. Distinctive features of the domain boundaries (some examples are indicated by arrows) are followed frame-by-frame in order to generate the velocity profile across the channel.

trance and exit of the channel.

The monolayer in the channel was viewed by means of a custom-built BAM. Light from a 30 mW 670 nm diode laser was p -polarized and directed onto the water surface at Brewster’s angle for water. The reflected light was focused onto a CCD camera by a $4\times$ microscope objective. An analyzing polarizer was inserted before the CCD array. The entire BAM could be translated to observe the flow at various places along the channel. In general, we found that the velocity profile was identical anywhere along the channel more than a few channel widths separated from the entrance or exit. We report the pattern of this fully developed flow. The molecular axis is tilted away from the surface normal in the L_2 phase and the azimuthal direction of the tilt is well-correlated over macroscopic distances (within a particular “domain”). BAM is sensitive to the anisotropy created by the molecular tilt, hence the monolayer appears as a mosaic of domains, each gray level corresponding to a different azimuthal tilt direction [15]. We used the naturally occurring distinctive shapes of the domain boundaries as markers to follow the monolayer during flow (see Fig. 2). Occasionally, small pieces of “collapsed” monolayer appearing in the image were also used as markers. We found that as long as the density of such pieces was small, the velocity profiles obtained were identical to those obtained in a monolayer with no collapsed pieces. The BAM image was videotaped and

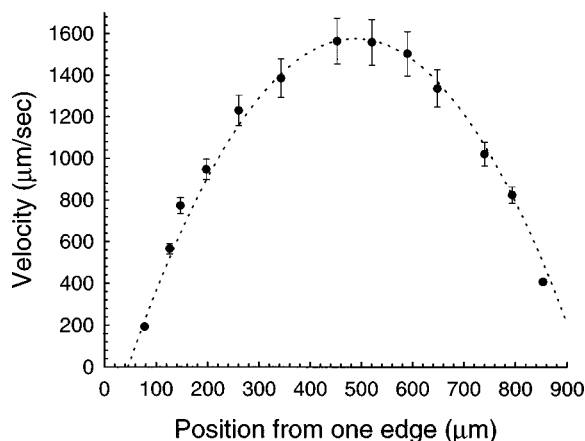


FIG. 3. Velocity profile during monolayer flow at $\pi = 18.0$ mN/m ($T = 21.5$ °C). The dashed line in this figure (and all other figures) represents the best parabolic fit to the data. The parabolic (Poiseuille) profile indicates that the interfacial viscosity dominates the drag due to subphase coupling and that the monolayer response is Newtonian.

later analyzed frame by frame in order to extract the velocity profile.

RESULTS

At values of surface pressure below 20 mN/m a parabolic velocity profile (see Fig. 3) was observed for reasonable values of shear rate. According to the paper by Stone [11], this implies that the surface viscosity $\mu_s > a\mu$, where $2a$ is the channel width (1 mm) and μ is the subphase viscosity. Therefore $\mu_s > 5 \times 10^{-4}$ g/s. (Stone notes that for lower values of surface viscosity, the profile begins to broaden and approach a more elliptical shape.) In fact, we show below that the surface viscosity in this system may be as high as 10^{-3} – 10^{-2} g/s. This parabolic (Poiseuille) profile is also consistent with a Newtonian fluid, the viscosity is shear rate-independent. Interestingly, at extremely high flow rates and low surface pressure the velocity profile becomes trapezoidal (see Fig. 4) with very steep sides. This corresponds essentially to “plug-flow” with the shear confined to a narrow

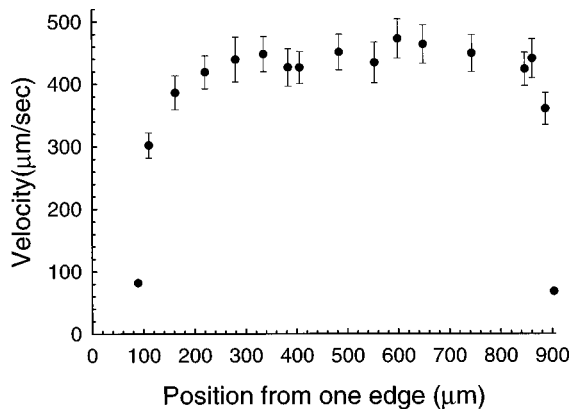


FIG. 4. Velocity profile during monolayer flow at $\pi = 12.5$ mN/m ($T = 21.5$ °C). The trapezoidal profile (plug flow) indicates shear-thinning response—the shear is confined to narrow layers near the edges. The profile at lower flow rates is similar to the parabolic one shown in Fig. 3.

boundary layer near the wall. This behavior is, of course, non-Newtonian, and is typical of shear-thinning—the viscosity decreases with increasing shear rate. Shear thinning has been previously observed in surfactant monolayers [1] and is not unusual in common liquids at high shear rates. We estimate the critical shear rate for the onset of the plug flow to be 5 s^{-1} , much higher than the critical shear rates for interfacial shear thinning usually reported of 10^{-3} – 10^{-2} s^{-1} [1].

At values of surface pressure above 20 mN/m, the velocity profile is again parabolic for low flow rates [see Fig. 5(a)]. However, a dramatically different scenario is observed with increasing flow rate—the profile gradually sharpens [Figs. 5(b) and 5(c)] until it becomes *triangular* [see Fig. 5(d)]. At still higher flow rates, the measured velocity profile continues to be approximately triangular up to the limit of our ability to observe the flow—about $500 \mu\text{m/s}$ [Fig. 5(e)]. In the case of the triangular profile, the shear rate is, of course, constant across most of the channel (the profile is slightly blunted near the center). The critical shear rate for the onset of the sharpened profile is in the range 0.06 – 0.27 sec^{-1} . This implies a relaxation time in the system of the order of 5 – 10 s.

The velocity profiles presented above are typical of those obtained in dozens of repetitions of the experiments. The flow behavior of the monolayer was indistinguishable at 20.5 °C and 21.5 °C. The behavior was qualitatively consistent at 23 °C, although we did not perform as detailed experiments at this temperature.

The surface pressure drop along the channel was measured as a function of flow rate. These drops were in the range 0.1 – 0.5 mN/m and were not of sufficient magnitude to cause a transition from the low pressure to high pressure regime or vice versa. In the following section we extract an effective surface viscosity as a function of shear rate from these data.

DISCUSSION

A blunted velocity profile generally indicates shear-thinning and a sharpened profile indicates shear-thickening. We have found it instructive to compare our experimental results to a common *ad hoc* model for non-Newtonian fluids, the power-law model [16]. In this model the constitutive equation is written as

$$\tau = K \left| \frac{du}{dx} \right|^{\alpha-1} \frac{du}{dx},$$

where τ is the shear stress, K is a constant, and du/dx is the rate of shear strain. A shear rate dependent, apparent viscosity is given by

$$\mu_{\text{app}} = K \left| \frac{du}{dx} \right|^{\alpha-1}.$$

This model is particularly convenient because it incorporates a wide variety of non-Newtonian behavior. For $\alpha < 1$ the model describes pseudoplastic (shear-thinning) behavior while for $\alpha > 1$ it describes dilatant (shear-thickening) response. For $\alpha = 1$ the model reduces to a simple Newtonian fluid with viscosity K . The velocity profile, for the geometry

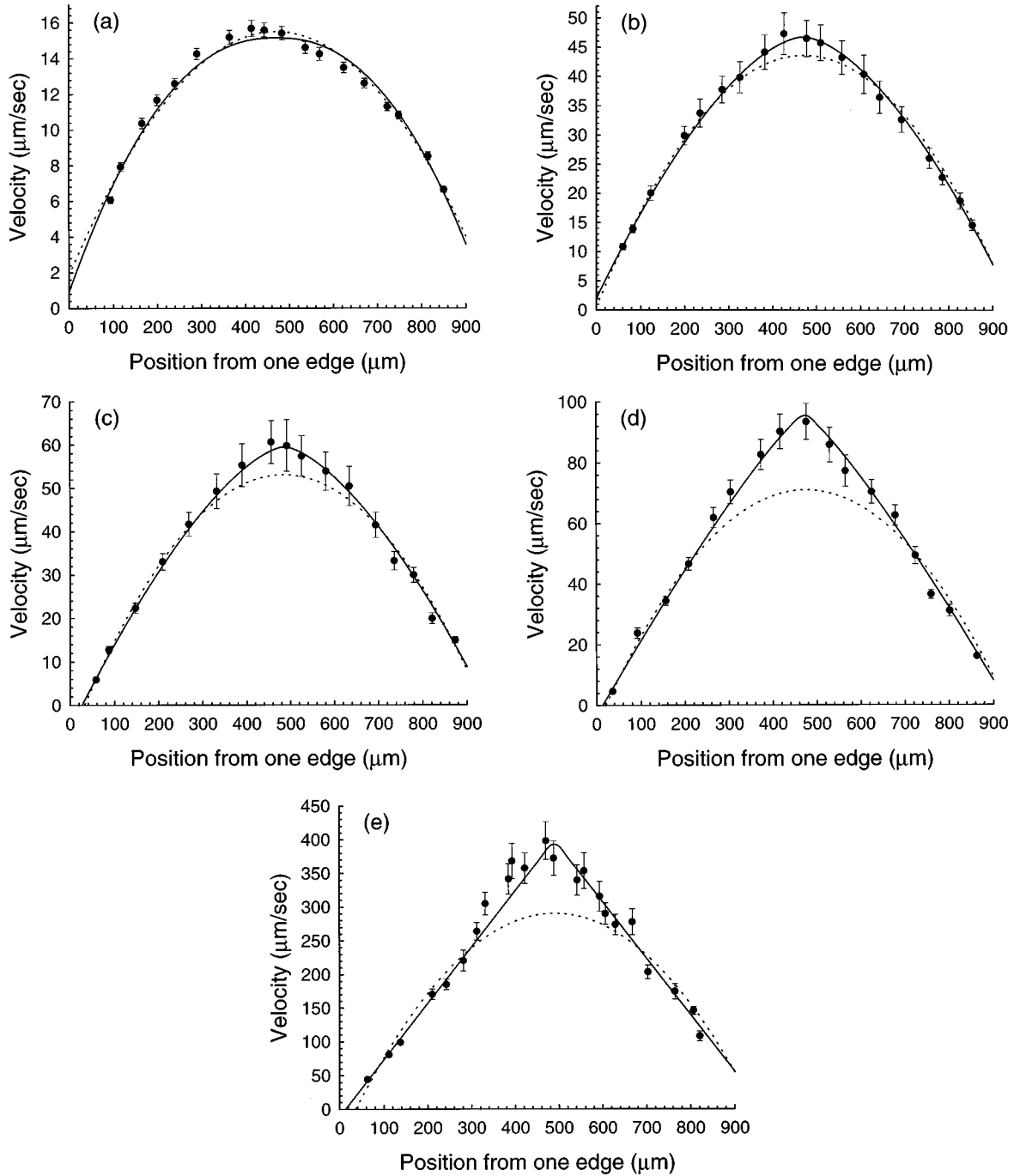


FIG. 5. Velocity profiles during monolayer flow at $\pi = 20.5$ mN/m ($T = 21.5$ °C) as the flow rate is increased. The dashed lines represent the best parabolic fit and the solid lines represent the best fit to a power law model (see text). (a) At low flow rates the profile is effectively parabolic, consistent with Newtonian response. (b)–(d) As the flow rate is increased the profile becomes sharper. The exponents α for the power law fits are as follows: (a) $0.77 (\pm 0.14)$, (b) $1.56 (\pm 0.12)$, (c) $1.9 (\pm 0.5)$, (d) $9 (-6, +\infty)$, (e) $182 (-171, +\infty)$.

of our experiment (neglecting subphase drag), for a two-dimensional power-law fluid is

$$u \propto \left[1 - \left(\frac{x}{a} \right)^{1+\alpha/\alpha} \right],$$

where a is the half-width of the channel and $x=0$ along the centerline of the channel. Figure 6 shows qualitatively the changes expected in the velocity profile for pseudoplastic, Newtonian, and dilatant fluids. Note that a triangular profile is observed as $\alpha \rightarrow \infty$, plug flow is approached as $\alpha \rightarrow 0$, and

a parabolic profile is obtained at $\alpha = 1$. Although we know of no *a priori* physical justification for this model, it nevertheless serves as a useful fitting function to help quantify our results.

We obtain reasonable fits to the experimental velocity profiles using the power-law model, as shown in Figs. 5(a)–5(d). For nearly triangular profiles ($\alpha > 3$), the fit becomes less sensitive to the value of the exponent [Fig. 5(d)]. In Fig. 7 we display the evolution of the experimental velocity profile with increasing flow rate in the high surface pressure regime. For clarity, we plot only the fits.

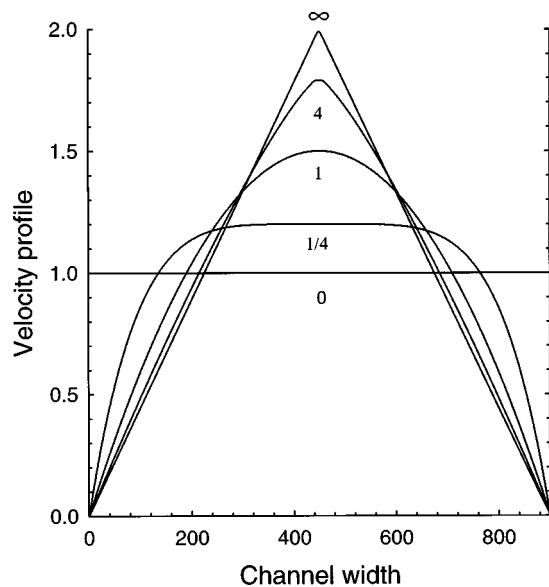


FIG. 6. Theoretical velocity profiles obtained using the *ad hoc* power law model. For an exponent, α , of unity, the model reduces to a Newtonian fluid, yielding a parabolic profile. For exponents less than unity (shear-thinning), the profile flattens out, approaching plug flow at $\alpha=0$. For exponents greater than unity (shear-thickening), the profile becomes sharper approaching a triangle at $\alpha=\infty$.

The sharpened velocity profiles observed at high flow rates above $\pi=20$ mN/m would seem to indicate shear thickening in the monolayer. The viscosity is defined as $\tau/(\partial u/\partial x)$; τ , the shear stress, varies linearly across the channel but the shear rate varies with a lower power. This implies that the viscosity increases towards the edges of the channel—at high shear rates. To be consistent with shear-thickening, the surface pressure drop along the channel

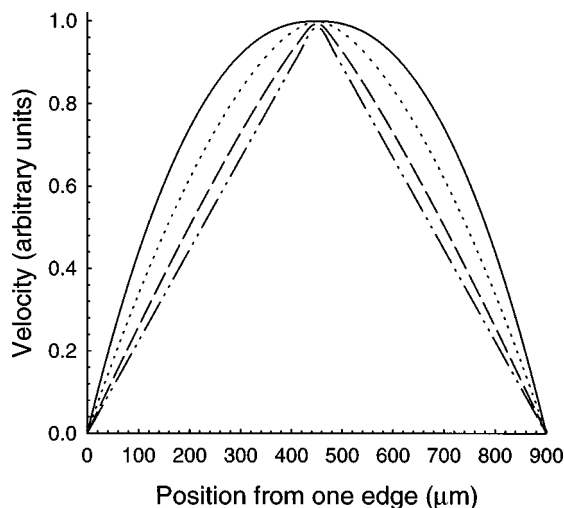


FIG. 7. Evolution of the measured velocity profiles for a monolayer at $\pi=20.5$ mN/m with increasing flow rate. The fits are scaled to have the same maximum and plotted without data points for clarity. The actual maximum velocities are as follows: solid line, $15.2 \mu\text{m/s}$; dotted line, $46.8 \mu\text{m/s}$; dashed line, $95.7 \mu\text{m/s}$; and dash-dotted line, $398.3 \mu\text{m/s}$.

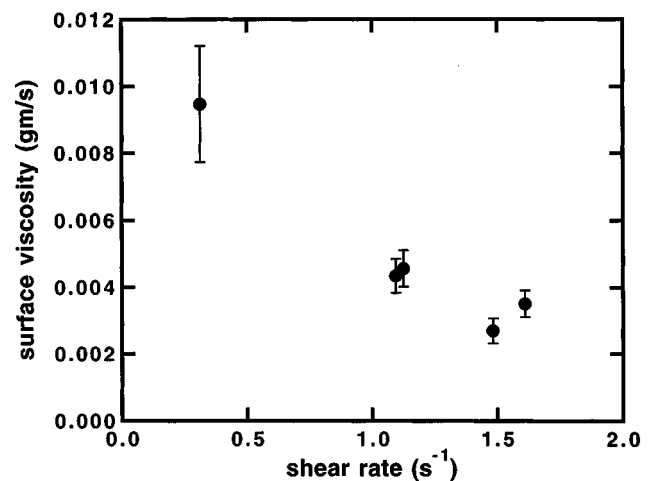


FIG. 8. A dimensionally correct approximation for the average surface viscosity in the channel is plotted versus the average shear rate over a range of flow rates where a sharpened velocity profile is observed. The quantity $(d\pi/dl)a^2/2u_{\text{max}}$ (exact for a Newtonian fluid) is used for the approximate surface viscosity and the average shear rate is taken as u_{max}/a , where $d\pi/dl$ is the surface pressure drop per unit length, a is the channel half-width, and u_{max} is the maximum velocity in the channel. These values of surface viscosity can be incorrect by a multiplicative factor of order unity; however, they can be safely compared to each other since the velocity profiles were similar. The plot demonstrates that the macroscopic shear viscosity decreases with shear rate.

should rise dramatically with flow rate—faster than the proportional rise expected for a Newtonian fluid. However, direct measurement of the surface pressure drop, in the regime where the profile is sharpened [see Figs. 5(d) and 5(e)], indicates that the surface viscosity is, in fact, decreasing with shear rate (see Fig. 8). We do not believe that this seeming paradox is due to experimental artifact for two reasons: (1) the results were reproducible in dozens of repetitions of the experiment over a period of about one year, using various individual channels and two different trough-barrier combinations; (2) the high flow rate behavior of the velocity profile undergoes a sharp change at $\pi=20$ mN/m, suggesting that the properties of the monolayer are responsible for the change. Instead, we speculate that the liquid-crystalline properties of the monolayer may affect the profile at high flow rates. The monolayer is not in an isotropic fluid state, but a liquid-crystalline mesophase (a hexatic phase). As the BAM images demonstrate, orientational correlations often extend hundreds of μm . Although continuum elastic theories for these 2D hexatic phases [17,18] have been extremely successful at describing distinctive static textures such as stripes [18,19] and star defects [20], we know of no attempt to couple this elastic theory to flow.

Since the monolayer is a complex system, there are several possible explanations for the time scale (5–10 s) corresponding to the onset of the velocity profile sharpening. A hexatic phase, like the fatty acid L_2 phase, can be thought of as a 2D crystalline phase with a high density of isolated lattice defects (dislocations). In our case, we also have a polycrystalline sample. Therefore, the likely candidates for relaxation processes include slippage along domain bound-

aries and motion of lattice defects within domains. Bruinsma *et al.* [21] calculated an approximate stress relaxation time for freely suspended films of hexatic liquid crystals that can be adapted for our system. The relaxation time due to domain slippage is $t = \mu_s L / \varepsilon w$, where L is the domain size (about 50 μm), ε is the shear modulus of the hexatic phase (on the order of 1–10 ergs/cm^2 [4,22]), μ_s and w are the surface viscosity and width, respectively, of the hypothetical 2D liquid layer presumed to lubricate the domain slippage (about 10^{-6} – 10^{-5} g/s [10,11] and about 5 \AA , respectively). Inserting these rough numbers gives a relaxation time in the range 0.01–1 s, close to the observed time scale at the high end. However, relaxation due to motion of dislocations within hexatic domains is also a possible source for the time scale. Since this relaxation time depends strongly on the dislocation density (an unknown quantity), it is difficult to estimate. We plan to extend these experiments to other hexatic monolayer phases and attempt to correlate the behavior with material parameters such as domain size, storage modulus, molecular tilt, etc. in an attempt to determine the true relaxation mechanism.

The sharpening of the velocity profile appears rather abruptly at surface pressure $\pi = 20$ mN/m . Below this pressure we do not observe the sharpening even for extremely high shear rates (see Fig. 3). This seems to imply a distinct change in the monolayer behavior at this pressure, perhaps a phase transition. This question is currently controversial. Tippman-Krayer *et al.*'s grazing incidence x-ray diffraction (GIXD) studies [23] of arachidic acid monolayers concluded that the L_2 phase (a mesophase in which the molecules are tilted towards their nearest neighbor) persists until the kink in the surface pressure vs area isotherm at about 24 mN/m . Their data established that the tilt angle varies smoothly as the monolayer is compressed. Interestingly, 20 mN/m corresponds to the tilt angle at which the in-plane lattice is approximately hexagonal. However, Peterson *et al.* [24] have reported the observation of a different phase for $\pi \geq 15$ mN/m —a chiral mesophase in which molecules are

tilted neither in the nearest-neighbor nor the next-nearest-neighbor direction. They did not, unfortunately, discuss the possible origins of the inconsistency of the two measurements and it is, therefore, difficult to know which picture to apply to the present experiments. In any case, our results are consistent with an abrupt change in the monolayer's rheological properties at $\pi = 20$ mN/m .

CONCLUSION

Direct observation of channel flow in a Langmuir monolayer of arachidic acid has proven to be a useful method for studies of interfacial rheology. In the L_2 mesophase, we have observed two distinct regions based on the monolayer rheology. At surface pressures below 20 mN/m , the monolayer behaves as a viscous two-dimensional Newtonian fluid, although at extremely high shear rates we observe plug flow. At $\pi > 20$ mN/m , however, the monolayer is Newtonian only for low shear rates, displaying dramatic sharpening of the velocity profile at shear rates greater than 0.2 s^{-1} . However, the surface-pressure drop across the channel as a function of flow rate is not consistent with shear-thickening behavior as indicated by the sharp velocity profile. The sharp change in monolayer rheology at $\pi = 20$ mN/m suggests that the monolayer undergoes a 2D phase transition at this surface pressure. These observations highlight the importance of direct flow visualization in addition to measurement of surface viscosity.

ACKNOWLEDGMENTS

We thank Gerry Fuller, Howard Stone, and Robijn Bruinsma for many helpful conversations. This work was supported by the Center for Photoinduced Processes (funded by the National Science Foundation and the Louisiana Board of Regents), the Louisiana Education Quality Support Fund Contract No. LEQSF(1996-99)-RD-B-12, and the Donors of the Petroleum Research Fund.

-
- [1] D. A. Edwards, H. Brenner, and D. T. Wasan, *Interfacial Transport Processes and Rheology* (Butterworth-Heinemann, Stoneham, MA, 1991).
- [2] W. D. Harkins and J. G. Kirkwood, *J. Chem. Phys.* **6**, 53 (1938).
- [3] L. E. Copeland, W. D. Harkins, and G. E. Boyd, *J. Chem. Phys.* **10**, 357 (1942).
- [4] B. M. Abraham, K. Miyano, S. Q. Xu, and J. B. Ketterson, *Phys. Rev. Lett.* **49**, 1643 (1982).
- [5] K. Miyano, B. M. Abraham, J. B. Ketterson, and S. Q. Xu, *J. Chem. Phys.* **78**, 4776 (1983).
- [6] H. Bercegol and J. Meunier, *Nature* **356**, 226 (1992).
- [7] J. T. Petkov, K. D. Danov, N. D. Denkov, R. Aust, and F. Durst, *Langmuir* **12**, 2650 (1996).
- [8] C. F. Brooks, G. G. Fuller, C. W. Frank, and C. R. Robertson (unpublished).
- [9] T. Maruyama, G. Fuller, C. Frank, and C. Robertson, *Science* **274**, 233 (1996).
- [10] D. K. Schwartz, C. M. Knobler, and R. Bruinsma, *Phys. Rev. Lett.* **73**, 2841 (1994).
- [11] H. A. Stone, *Phys. Fluids* **7**, 2931 (1995).
- [12] D. Hönig and D. Möbius, *J. Phys. Chem.* **95**, 4590 (1991).
- [13] S. Hénon and J. Meunier, *Rev. Sci. Instrum.* **62**, 936 (1991).
- [14] C. M. Knobler and R. C. Desai, *Annu. Rev. Phys. Chem.* **43**, 207 (1992).
- [15] S. Hénon and J. Meunier, *J. Phys. Chem.* **98**, 9148 (1993).
- [16] S. W. Churchill, *Viscous Flows: The Practical Use of Theory* (Butterworth, Stoneham, MA, 1988).
- [17] J. V. Selinger, Z.-G. Wang, R. F. Bruinsma, and C. M. Knobler, *Phys. Rev. Lett.* **70**, 1139 (1993).
- [18] D. K. Schwartz, J. Ruiz-Garcia, X. Qiu, J. V. Selinger, and C. M. Knobler, *Physica A* **204**, 606 (1994).
- [19] J. Ruiz-Garcia, X. Qiu, M.-W. Tsao, G. Marshall, C. M. Knobler, G. A. Overbeck, and D. Möbius, *J. Phys. Chem.* **97**, 6955 (1993).
- [20] X. Qiu, J. Ruiz-Garcia, K. J. Stine, C. M. Knobler, and J. V.

- Selinger, Phys. Rev. Lett. **67**, 703 (1991).
- [21] R. Bruinsma, B. I. Halperin, and A. Zippelius, Phys. Rev. B **25**, 579 (1982).
- [22] M. Yazdanian, H. Yu, G. Zograf, and M. W. Kim, Langmuir **8**, 630 (1992).
- [23] P. Tippmann-Krayer and H. Möhwald, Langmuir **7**, 2303 (1991).
- [24] I. R. Peterson, R. M. Kenn, A. Goudot, P. Fontaine, F. Rondelez, W. G. Bouwman, and K. Kjaer, Phys. Rev. E **53**, 667 (1996).